

POSTIRRADIATION DEFORMATION MICROSTRUCTURES IN FERRITIC Fe-9Cr - D. S. Gelles, M. L. Hamilton (Pacific Northwest National Laboratory) and R. Schäublin (EPFL-CRPP Fusion Technology, Switzerland)

OBJECTIVE

The objective of this effort is to provide further understanding of postirradiation deformation mechanisms controlling in ferritic/martensitic steels.

SUMMARY

The deformed microstructures of both irradiated and unirradiated Fe-9Cr uniaxial tensile specimens have been examined to identify controlling mechanisms. Deformation following irradiation is found to occur in poorly defined channels, causing formation of discrete steps at surfaces and delineated by nonuniformly distributed highly elongated voids. Deformation is by motion of $\frac{1}{2}\langle 111 \rangle$ dislocations, which interact with and decompose irradiation-induced $a\langle 100 \rangle$ loops. The structure formed after extensive deformation consists of highly complex cell walls and moderate densities of individual slip dislocations.

PROGRESS AND STATUS

Introduction

Post-irradiation deformation behavior on a microstructural scale in ferritic/martensitic steels represents an important field for research that has been largely ignored. This is in part due to limitations imposed by specimen availability, imaging challenges, and as will be shown, localized flow limitations. We have previously attempted to examine postirradiation deformation in Fe-6Cr and -12Cr specimens, without success [1], but are unaware of any other similar efforts. In this previous attempt, specimens of deformed miniature sheet tensile specimens were prepared about 1.5 mm from the fracture surface, but the microstructures found were characteristic of undeformed material. This topic is of importance because martensitic steels are considered candidate materials for fusion structural applications, and postirradiation deformation in general, and embrittlement in particular are expected to define the low temperature limits for application. The topic is of particular interest because ferritic steels provide an unusual example where irradiation produces a Burger's vector ($a\langle 100 \rangle$) that is not normally encountered in unirradiated ferritic steels, nor is it found in most other body centered cubic metals. Also, it is not clear how slip dislocations of type $\frac{1}{2}\langle 111 \rangle$ can interact with $a\langle 100 \rangle$ Burger's vectors so as to annihilate all $a\langle 100 \rangle$ segments.

Experimental Procedures

Miniature sheet tensile specimens of Fe-Cr alloys were irradiated in fusion irradiations in the FFTF, and were tested to provide understanding of postirradiation deformation response in simple alloys [1,2]. Later irradiation experiments duplicated these conditions, but did not exceed them because FFTF was shut down prematurely. Because the conditions were duplicates, they were ignored and deformation testing was terminated. From the available specimen conditions, the two listed in Table 1 were easily accessible and were chosen for study. It was decided to limit the present study to Fe-9Cr (Fe-9.6Cr-0.002C-0.022O-

*Pacific Northwest National Laboratory (PNNL) is operated for the U.S. Department of Energy by Battelle Memorial Institute under contract DE-AC06-76RLO-1830.

0.0017N in wt% [3]) in order to best match the low activation candidate alloy compositions. This meant that two specimens were available from capsule ZP-1 and four were available from ZR1. Unirradiated control duplicates could not be found, so SS-3 control samples with identical heat treatment were substituted to provide control condition microstructures.

Table 1. Irradiation Conditions for miniature sheet tensile specimens.

Capsule ID	MOTA/Basket	Irr. Temp (°C)	Fluence (n/cm ²)	Dose (dpa)
ZP1	1E/BCB-1	370	2.79x10 ²²	10.4
ZR1	1E/2C-3	403	9.46x10 ²²	40.5

Specimen flats were mechanically polished to Linde 600 grit and deformed at room temperature either to failure on the first test or to ~2% for the irradiated specimens and ~8% for the unirradiated specimens using procedures previously described [2]. Testing details are given in Table 2 with elongations estimated from test traces. If uniform elongation (UE) and total elongation (TE) are not provided, the test was stopped prior to failure.

Table 2. Test Details for Deformed Tensile Specimens.

Specimen ID	Condition	YS (MPa)	UTS (MPa)	Elongation (%)
6721	unirradiated	194	326	16.4 UE, 27.3 TE
6720	"	139	250	8.5
6724	"	142	239	7.2
ZR01	40 dpa at 403	534	534	0.02 UE, 4.1 TE
ZR02	"	540	554	2.3
ZP01	10 dpa at 370	619	619	2.6

Maximum load response as shown in reference 2, page 1240.

Following deformation, specimens were examined by SEM to identify regions that were deformed. Unirradiated SS-3 specimens were then ground from 0.030" (0.75 mm) to about the thickness of the miniature specimens: 0.010" (0.25 mm). Disks 1 mm in diameter were then punched from promising areas so that the edge of the specimen was retained on one side to allow determination of the stress axis. Each disk was then mounted in a 3 mm stainless steel disk using recently developed procedures [4] and prepared using normal polishing procedures. TEM was performed on a JEOL 1200EX transmission electron microscope operating at 120 KeV and using a double tilting ±45° goniometer stage. Imaging included procedures for identifying each of the $a\langle 100 \rangle$ and $\frac{1}{2}\langle 111 \rangle$ Burgers vectors in a field of view [5]. All micrographs were digitized and stereo images were prepared as anaglyphs, available on request.

Results

Surface Features

SEM revealed that surfaces of both irradiated and unirradiated specimens had developed clearly defined steps. The vertical surfaces of these steps were not flat, but instead showed fine structure. However, the irradiated specimens showed no other features whereas the unirradiated specimens developed more rounded step edges and more structure on the original surfaces. Examples are provided in Figures 1 and 2. Figure 1 compares the specimens at low magnification and Figure 2 shows examples of specimen surfaces at higher magnifications.

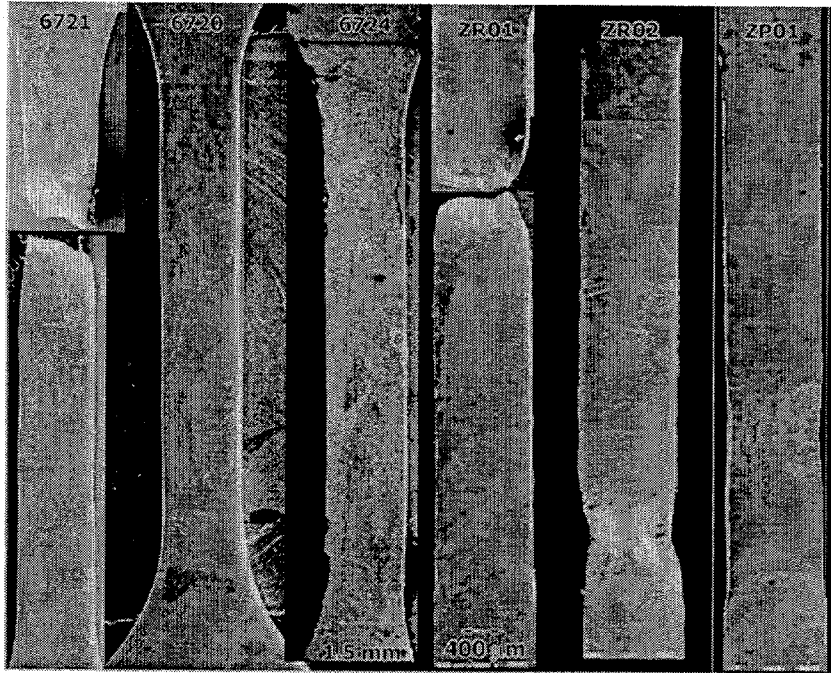


Figure 1. Low magnification examples of deformed tensile specimens with unirradiated specimens on the left. Note differences in magnification.

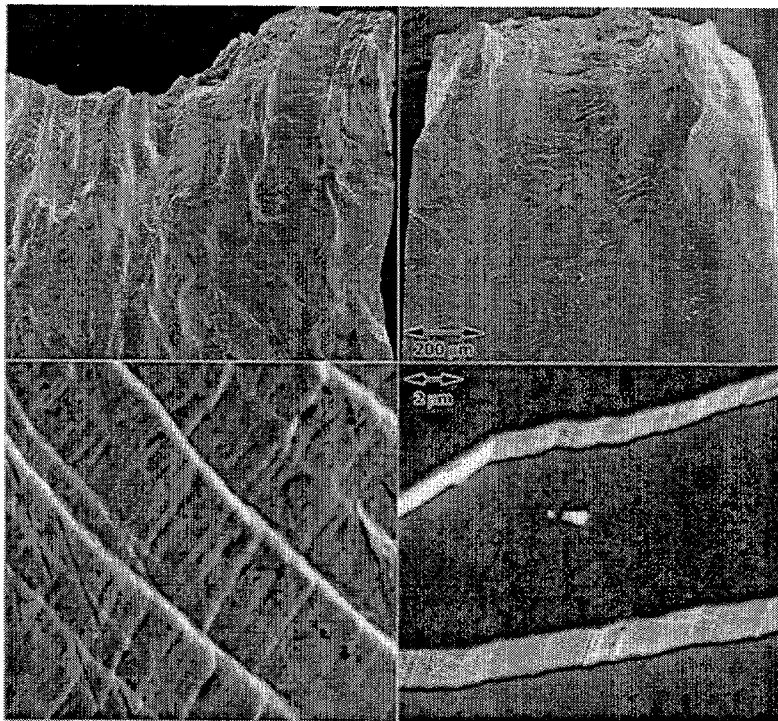


Figure 2. Higher magnification examples of the fracture surfaces and slip steps, with the unirradiated condition on the left.

Figure 1 shows the unirradiated specimens on the left and the irradiated samples on the right at decreasing strain from left to right. From Figure 1 it can be shown that strain is much more localized following irradiation. In fact, specimen ZP02, second from right is about to fail in the necked region with little indication of deformation elsewhere. Slip steps can be identified in the gauge sections only towards the grips, even in the failed specimen. From this figure, the reason for the previous inability to find deformation in reference 1 microstructural studies is apparent; deformation is so localized that material 1.5 mm from the fracture surface shows few slip steps. Deformation in the unirradiated specimens is much more uniform.

Figure 2 shows the fracture surfaces at higher magnification with unirradiated specimen 6721 on the left and irradiated specimen ZR01 on the right. Dimple rupture is apparent on the fracture surface following irradiation. The grain size is on the order of 200 μm and each grain contains slip steps appearing as wavy lines, but these lines are difficult to resolve in the unirradiated condition at lower magnification. Slip step spacing increases with distance from the fracture surface. At higher magnification in the lower images, it is apparent that in the irradiated case, the surface is stepped with no features on the original surface and fine structure on the step surfaces. In general, the fine structure is ridged, but several examples can be found where steps appear on this surface. Therefore, once deformation initiates on a plane, it tends to continue without change on that plane. In comparison, the unirradiated sample shows undulations on the original surface, step edges that are rounded and step surfaces that are more uneven. (Scratches are on the lower left and should be ignored.) Therefore, in the unirradiated case, deformation is less restricted to deformation channels.

Microstructural Examination

The unirradiated deformed condition was found to contain a moderate density of straight screw $\frac{1}{2}\langle 111 \rangle$ dislocation line segments, but $\frac{1}{2}\langle 111 \rangle$ loops produced by deformation were also found. An example demonstrating procedures that allow identification of all $\frac{1}{2}\langle 111 \rangle$ Burgers vectors, is given in Figure 3 for an area in specimen 6724 deformed approximately 7%. Figure 3 provides comparison of the same area imaged using $\bar{g}=01\bar{1}$ (vertical) in Figure 3a and 200 (horizontal) in Figure 3b taken near (011) orientations and $\bar{g}=10\bar{1}$ (with \bar{g} as shown) in Figure 3c taken near (131) [5]. In Figure 3a only $\frac{1}{2}[1\bar{1}\bar{1}]$ and $\frac{1}{2}[\bar{1}1\bar{1}]$ are in contrast, in Figure 3b, all $\frac{1}{2}\langle 111 \rangle$ dislocations are in contrast and in Figure 3c, only $\frac{1}{2}[\bar{1}\bar{1}1]$ and $\frac{1}{2}[\bar{1}1\bar{1}]$ are in contrast. Therefore, those dislocations that appear in Figures 3a and 3b, but not in 3c that tend to lie on the diagonal from lower left to upper right are of type $\frac{1}{2}[1\bar{1}\bar{1}]$ and are of screw configuration. A small loop, most visible in Figure 3a and marked with an arrow, appears to be an edge loop with $\frac{1}{2}[\bar{1}\bar{1}1]$ Burgers vector.

Except in samples that were taken where necking was occurring, the microstructures observed in irradiated samples were typical of the as-irradiated structure, as found in earlier work [1]. That structure consisted of equiaxed voids, $a\langle 100 \rangle$ loops, $\frac{1}{2}\langle 111 \rangle$ line segments, and perhaps large $\frac{1}{2}\langle 111 \rangle$ loops. Examples are provided in Figure 4 from specimens ZP01 away from the necked area and ZR01 near the fracture surface, showing bright field images with $\bar{g}=01\bar{1}$ (horizontal) and 200 (vertical) taken near (011) orientations, the lower dose and temperature on the left. For Figure 4, it can be noted that in $\bar{g}=200$ contrast, all $\frac{1}{2}\langle 111 \rangle$ dislocations are weakly visible and one set of $a\langle 100 \rangle$ are visible in strong contrast, those on the (200) plane, whereas in $\bar{g}=01\bar{1}$ contrast, only two sets of $\frac{1}{2}\langle 111 \rangle$ dislocations and the remaining $a\langle 100 \rangle$ dislocations are visible (with $a[100]$ invisible) [1,5]. Therefore, Figure 4 shows loops on the order of 50 nm predominantly of $a\langle 100 \rangle$ type with a few $\frac{1}{2}\langle 111 \rangle$ dislocation segments. Similar response was previously reported in undeformed specimens [1,3,6-8].

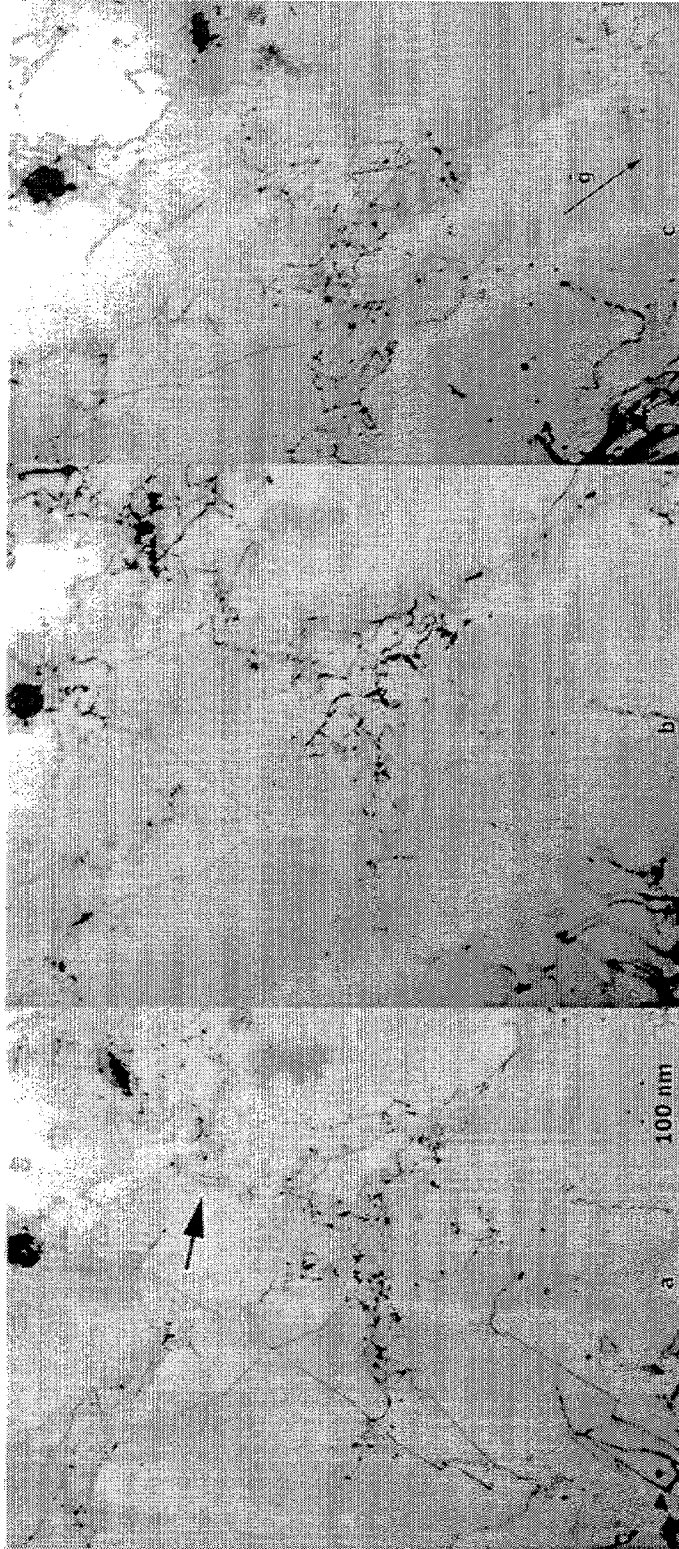


Figure 3 Dislocation structure in unirradiated deformed sample 6724.

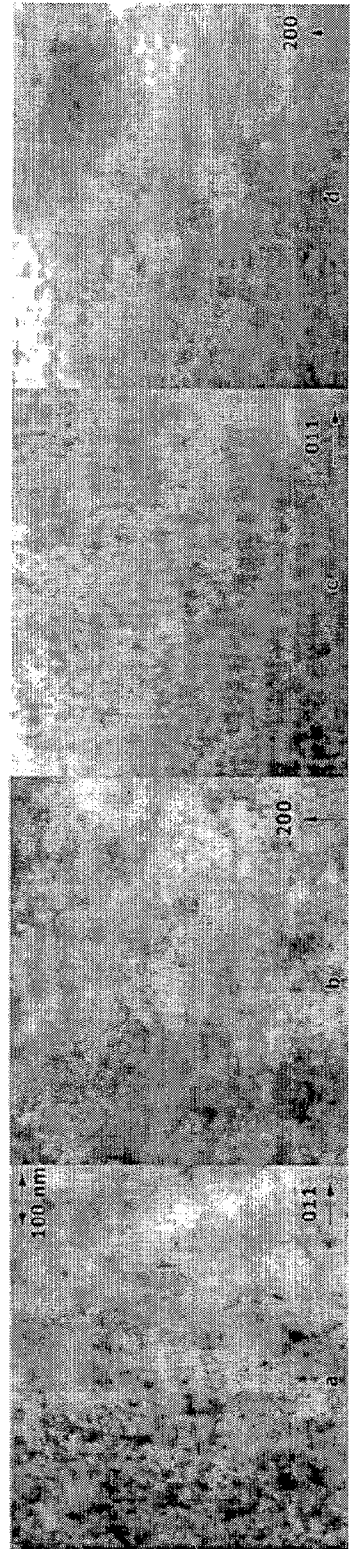


Figure 4. Microstructures in apparently undeformed regions for ZP01 in a) and b) and ZR01 in c) and d).

Figure 5 provides an example of the structure found in a deformed region of specimen ZR02, under various imaging conditions: $\bar{g}=01\bar{1}$ (horizontal), 200 (vertical) and in void contrast taken near a (011) orientation. From Figure 5, it can be noted that the contrast from $a\langle 100 \rangle$ dislocations is very different from that in Figure 4, in that voids are often linked to dislocations, and many examples of highly elongated voids can be identified. Therefore, postirradiation deformation effectively removes the $a\langle 100 \rangle$ loops created by irradiation but strain is very nonuniform, resulting in severe distortion of many voids but negligible distortion of neighboring voids.

The imaging procedures that allow identification of all $\frac{1}{2}\langle 111 \rangle$ Burgers vectors were applied to postirradiation deformation structures with less success because lattice rotation due to localized deformation was more severe and because $a[100]$ Burgers vectors are present. Examples are given in Figures 6 and 7. Both use the same imaging conditions as those used in Figure 3 with $\bar{g}=01\bar{1}$ horizontal in a and 200 vertical in b taken near (011) orientations but with either $\bar{g}=1\bar{1}0$ or $10\bar{1}$ (with \bar{g} as shown) in c taken near (113) or (131), respectively [5]. In Figures 6a and 7a, only $\frac{1}{2}[1\bar{1}1]$, $\frac{1}{2}[11\bar{1}]$, $a[010]$ and $a[001]$ dislocations are in contrast, in Figure 6b, all $\frac{1}{2}\langle 111 \rangle$ dislocations and $a[100]$ dislocations are in contrast, in Figure 6c, only $\frac{1}{2}[\bar{1}11]$, $\frac{1}{2}[1\bar{1}1]$, $a[100]$ and $a[010]$ dislocations are in contrast and in Figure 7c, only $\frac{1}{2}[\bar{1}11]$, $\frac{1}{2}[11\bar{1}]$, $a[100]$ and $a[001]$ dislocations are in contrast. Figure 6 was selected to show behavior in an early stage of deformation and Figure 7 to show more advanced stages of development. Examination of Figure 6 demonstrates structure at the lower left with several features similar to that shown in Figure 3, consisting of $a\langle 100 \rangle$ loops. However, much of this structure appears different, indicating that many of the $a\langle 100 \rangle$ loops have been altered. Other regions of Figure 6 are quite different in that no $a\langle 100 \rangle$ loops remain. Therefore, early in the deformation process, it is possible to remove the $a\{100\}$ loop structure.

Figure 7 indicates that later in the deformation process the dislocation structure coarsens and develops subgrain structure. Dislocations are found to be predominantly of $\frac{1}{2}[111]$ Burgers vector type and of screw configuration. The subgrain boundaries appear to be linked to void structure and are non-planar as indicated by the subgrain structure appearing on the left center of Figure 7a. However, the major deformation channels, as defined by the presence of highly elongated voids, are not parallel to nearby subgrain boundaries.

Discussion

It is now apparent that this work was only possible because novel specimen miniaturization procedures have been developed. Deformation in irradiated specimens is extremely localized, at least for the miniature specimens used in this study. Furthermore, it is straightforwardly possible to relate the dislocation structure available for analysis with reference to the tensile direction. However, no attempt has yet been made to relate Burgers vector anisotropy to the stress state. Instead, the emphasis was placed on understanding the dislocation reactions that lead to alteration of the irradiation induced dislocation structure and channel deformation.

Deformation is found to remove irradiation induced $a[100]$ edge dislocation loops. That process can be envisioned as follows.

A moving $\frac{1}{2}\langle 111 \rangle$ dislocation with the correct sense will interact with an $a\langle 100 \rangle$ loop according to the following reaction:

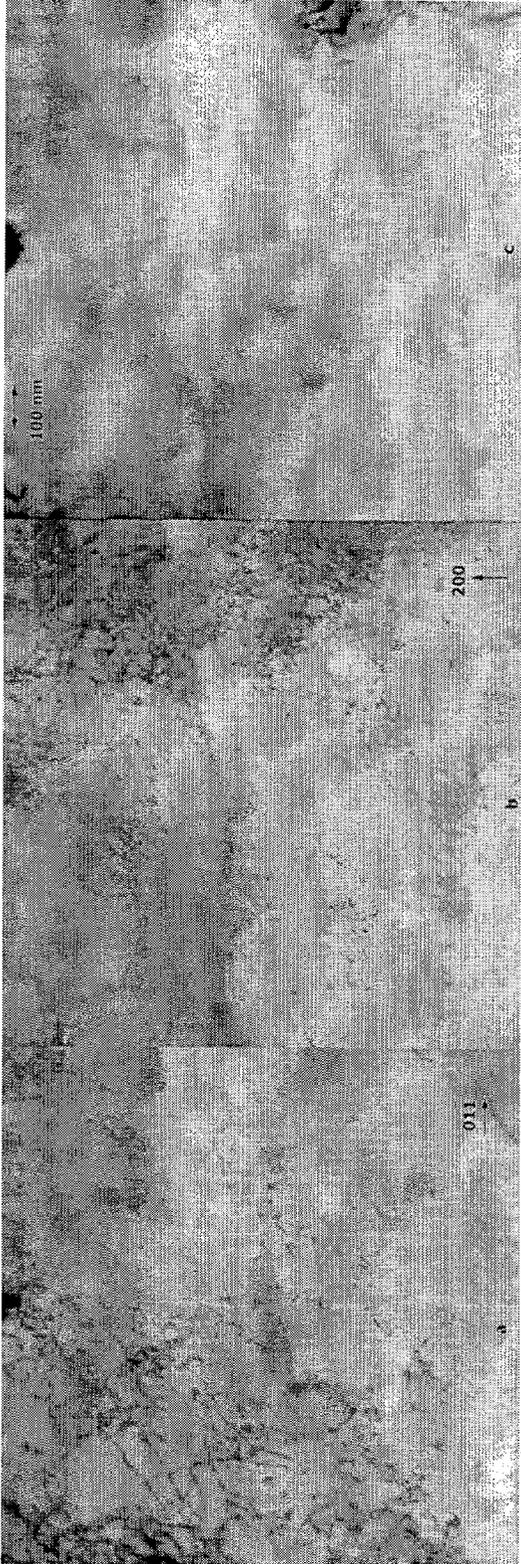


Figure 5. Microstructures in a deformed region of ZP02 in 011 (horizontal), 200 (vertical) and void contrast.

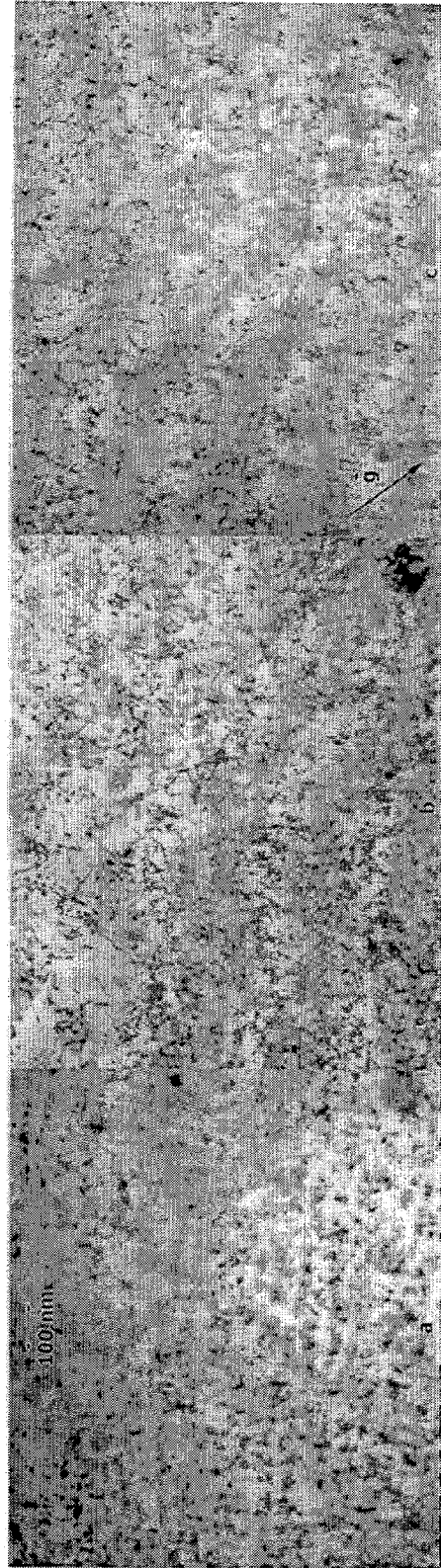


Figure 6. Microstructures in the necked region of irradiated condition ZP01 in 011 (horizontal), 200 (vertical) and 110 (as shown).

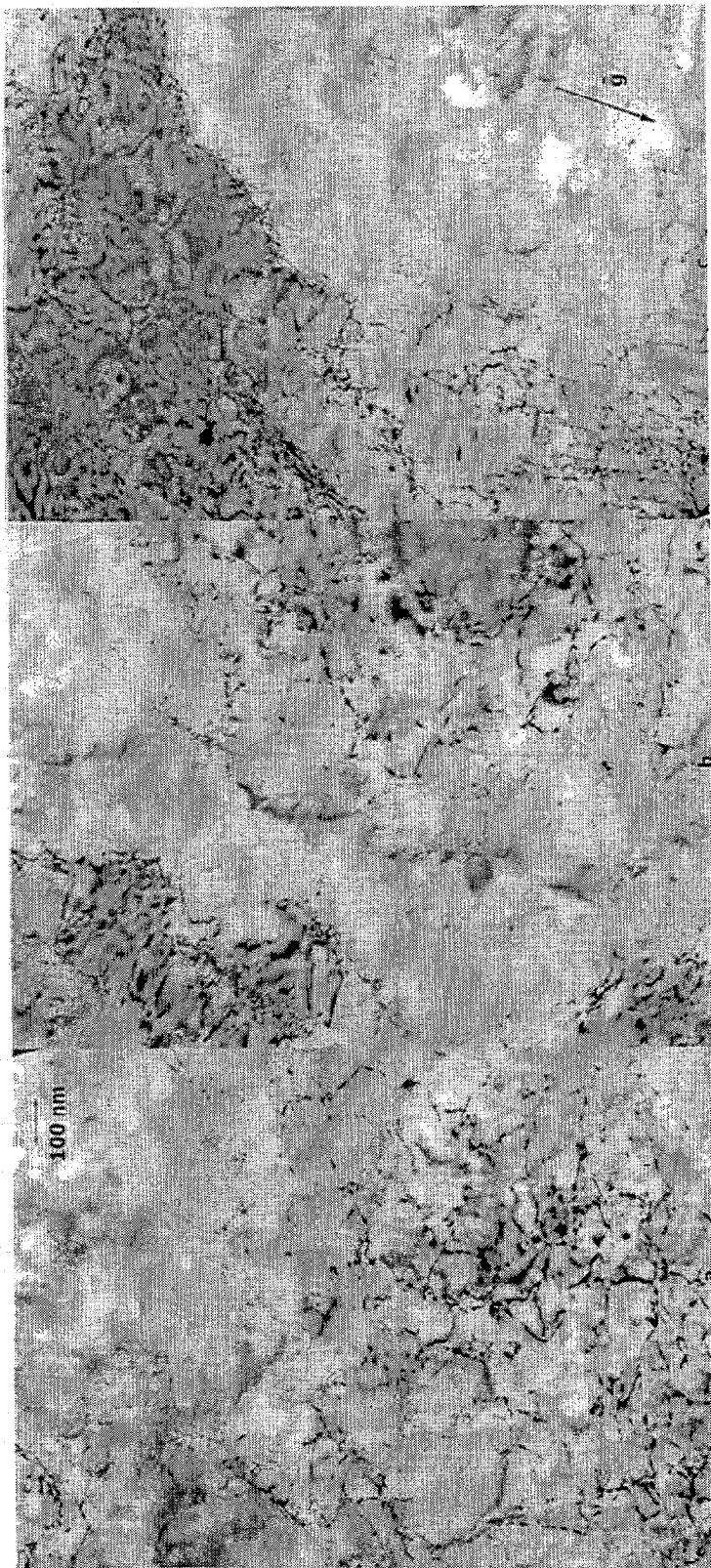


Figure 7. Microstructures in the necked region of irradiated condition ZR02 in $01\bar{1}$ (horizontal), 200 (vertical) and $10\bar{1}$ (as shown).

$$\frac{a}{2}[\bar{1}11] + a[100] = \frac{a}{2}[111]$$

Replacement of a section of the $a[100]$ loop with an $\frac{a}{2}[111]$ line segment therefore can take place with significant reduction in energy. This process can be expected to continue rapidly, replacing the $a[100]$ loop with an $\frac{a}{2}[111]$ loop lying on the (100) plane. This replacement reaction can occur with any moving $\frac{a}{2}\langle 111 \rangle$ dislocation but its sense will determine which side of the $a[100]$ loop it will be attracted to. Stereoscopic examination of features in Figure 6b reveals however that most of the $\frac{a}{2}\langle 111 \rangle$ loops present are not on {100} planes, and therefore, once formed, the loops are able to glide to more favorable configurations.

Reduction in dislocation density then occurs with further interaction between the newly formed $\frac{a}{2}\langle 111 \rangle$ loops and moving dislocations of similar Burgers vector. However, interactions between $\frac{a}{2}\langle 111 \rangle$ loops and dislocations of a different Burgers vector will not be energetically favorable, representing the reverse of the above interaction, and therefore, such loops will represent barriers to dislocation slip.

It is apparent that with sufficient deformation, all irradiation induced loops can be destroyed, leaving a dislocation structure with screw component characteristics similar to those created in deformed unirradiated conditions. Even after the irradiation-induced dislocation structure is removed, localized deformation continues, resulting in a higher density of surface steps and a transition into necking response. This may be a consequence of favorable dislocation nucleation or enhanced dislocation glide because the remaining microstructural obstacles to dislocation glide, the voids, are distorted.

It has been shown that some voids are elongated or, at least, deformed from the original equiaxed and faceted shape. The deformed elongated cavities are located in regions that form narrow bands that are about 100 nm wide as shown in Figure 8. The analysis of the shape of the elongated cavities allowed measurement of localized strains. The local strain is given by the ratio of length of the cavity, measured from top to bottom in the direction of the strain, and the original size, as measured by the size of the cavity at mid-height perpendicular to the strain axis. The average strain for highly elongated voids is about 300%, which represents the passage across a 25 nm cavity of about 100 dislocations.

Even though these bands are poorly defined, they clearly indicate deformation of the material occurring by localized shear. When these bands are correlated with the stepped traces revealed by the SEM analysis, it is clear that the irradiated material can deform via a channeling mechanism. Although channeling has been demonstrated in a number of irradiated fcc and ferritic materials [9-10], this is to our knowledge the first evidence for this mechanism in a Fe-9Cr type ferritic alloy.

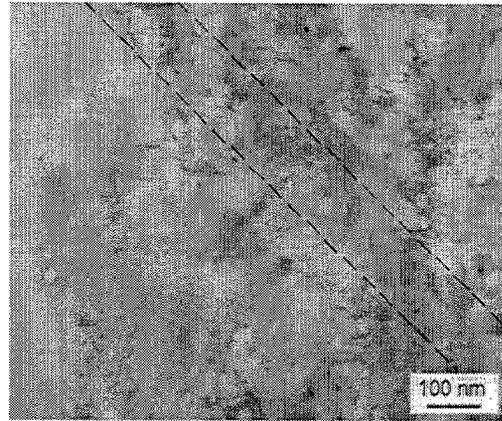


Figure 8. Microstructure in the necked region of irradiated condition ZR02 showing typical elongated cavities in poorly defined narrow bands. A band is delineated by the dashed lines.

Conclusions

A novel specimen preparation procedure has made it possible to examine postirradiation deformation in Fe-9Cr miniature sheet tensile specimens. It is found that

- 1) Deformation in irradiated specimens is highly localized so that specimens prepared more than 1 mm from the fracture surface usually showed no effects of deformation.
- 2) Surface slip steps created during postirradiation deformation are clearly defined with no other apparent surface damage whereas in unirradiated specimens the steps are more poorly defined and other surfaces show evidence of local deformation. The surface steps in irradiated specimens are nonplanar but features created early in the deformation are reproduced during further deformation creating ridges on the steps that are rarely altered with further deformation. Therefore, once localized slip is established in irradiated specimens, it generally continues without change. Localized necking occurs in irradiated specimens as slip steps get larger and slip planes increase in density.
- 3) Transformation of $a\langle 100 \rangle$ loops created during irradiation of ferritic alloys appears to proceed easily based on observed rapid disappearance of such features. It is proposed that this transformation is based on the reaction

$$\frac{1}{2}[\bar{1}11] + a[100] = \frac{1}{2}[111]$$
- 4) Continued postirradiation deformation removes all irradiation induced dislocation structure, replacing it eventually with $\frac{1}{2}[111]$ screw dislocations typical of deformation in unirradiated specimens.
- 5) Evidence for highly localized plasticity is found in the void structure so that some voids become highly elongated but nearby voids remain undistorted. Strains as high as 300% were identified in narrow bands that are about 100 nm wide. The controlling deformation mechanism is by channeling.
- 6) As local strains increase during postirradiation deformation, highly defined subgrain structure develops, whereas such structure is not found in unirradiated specimens deformed to about 8% uniform elongation.

FUTURE WORK

This work will be continued as needed.

REFERENCES

- [1] M. L. Hamilton, D. S. Gelles, and P. L. Gardner in Effects of Radiation on Materials: 16th International Symposium, ASTM STP 1175, A. S. Kumar, D. S. Gelles, R. Nanstad and E. A. Little, Eds., ASTM Philadelphia (1993) 545.
- [2] M. L. Hamilton and D. S. Gelles in Effects of Radiation on Materials: 15th International Symposium, ASTM STP 1125, R. E. Stoller, A. S. Kumar, and D. S. Gelles, Eds., ASTM, Philadelphia (1992) 1234.
- [3] D. S. Gelles, J. Nucl. Mater., 108 & 109 (1982) 515.
- [4] D. S. Gelles, S. Ohnuki, K. Shiba, Y. Kohno, A. Kohyama, J. P. Robertson, and M. L. Hamilton, in DOE/ER-0313/25 (1999) 143.

- [5] D. S. Gelles, A. Kimura and T. Shibayama in Effects of Radiation on Materials: 19th International Symposium, ASTM STP 1366, M. L. Hamilton, A. S. Kumar, S. T. Rosinski and M. L. Grossbeck, Eds. ASTM, W. Conshohocken, PA (2000) 535.
- [6] D. S. Gelles in Effects of Radiation on Materials: 14th International Symposium, Vol. 1, ASTM STP 1046, N. H. Packan, R. E. Stoller and A. S. Kumar, Eds., ASTM, Philadelphia 1990, 73-97.
- [7] D. S. Gelles, IBID Reference 1, 66.
- [8] D. S. Gelles, J. Nucl. Mater., 225 (1995) 163.
- [9] R. L. Fish, J. L. Straalsund, C. W. Hunter, and J. J. Holmes in Effects of Radiation on Substructure and Mechanical Properties of Metals and Alloys, ASTM STP 529, ASTM 1973, 149-164.
- [10] M. Victoria, N. Baluc, C. Bailat, Y. Dai, M.I. Luppó, R. Schäublin, B.N. Singh, J. Nucl. Mater., 276 (1-3) (2000) 114-122.